Journal of Solid State Chemistry **156,** 110–116 (2001)
doi:10.1006/jssc.2000.8969, available online at http://www.idealibrary.com on IDEAL®

Examination of the Anisotropic Spin Exchange Interactions of CuM_2O_6 (M = Sb, V, Nb) by Spin Dimer Analysis

H.-J. Koo and M.-H. Whangbo[1]

Department of Chemistry, North Carolina State University, Raleigh, North Carolina 27695-8204

Received May 12, 2000; in revised form August 17, 2000; accepted September 15, 2000; published online December 21, 2000

The anisotropic spin exchange interactions of the magnetic solids CuM_2O_6 (M = Sb, V, Nb) were explained by analyzing their reported crystal structures and calculating the spin orbital interaction energies of their spin dimers. The magnetic orbital of each Cu^{2+} site in CuM_2O_6 is given by the "x^2–y^2" orbital so that the magnitude of an antiferromagnetic spin exchange interaction for a given spin dimer increases when the arrangement of the nearest-neighbor square-planar CuO_4 units containing the magnetic orbitals provides a good sigma overlap between the adjacent magnetic orbitals. The one-dimensional magnetic chains of α-CuV_2O_6, β-$CuNb_2O_6$, and α-$CuNb_2O_6$ run along a direction different than their edge-sharing CuO_4 chain directions. Our study predicts that the antiferromagnetic ordering in β-$CuNb_2O_6$ should make the magnetic unit cell double the chemical unit cell along the *b*-direction. © 2001 Academic Press

1. INTRODUCTION

The magnetic properties of the compounds CuM_2O_6 (M = Sb, V, Nb) originate from the Cu^{2+} (d^9) ions because the other ions M^{5+} and O^{2-} (from the viewpoint of the ionic electron counting) are diamagnetic. The structures of CuM_2O_6 are made up of distorted CuO_6 and MO_6 octahedra. In $CuSb_2O_6$ the CuO_6 octahedra are separated from one another, but the magnetic susceptibility of $CuSb_2O_6$ is well described by the one-dimensional (1D) Heisenberg antiferromagnetic (AFM) chain model (1). The α-CuV_2O_6 phase, in which the CuO_6 octahedra form *trans*-edge-sharing CuO_4 linear chains (2), exhibits a 1D short-range AFM ordering with the susceptibility maximum at $T_M = 44$ K and undergoes a three-dimensional (3D) AFM ordering at $T_N = 24$ K (3). In both α-$CuNb_2O_6$ (4–6) and β-$CuNb_2O_6$ (5–7), the CuO_6 octahedra from *cis*-edge-sharing CuO_4 chains. β-$CuNb_2O_6$ shows a 1D short-range AFM ordering with $T_M = 20$ K(8) and a 3D AFM ordering at $T_N = 7.5$ K (9). In contrast, α-$CuNb_2O_6$ is a spin gap system and its magnetic susceptibility, though analyzed earlier by an isolated spin dimer model (5), is better described by an alternating 1D AFM chain model (10). Thus, all the CuM_2O_6 (M = Sb, V, Nb) phases have a 1D magnetic chain character.

The anisotropic spin exchange interactions of a magnetic solid are described by the spin exchange parameters J of the spin Hamiltonian employed to reproduce the temperature-dependent magnetic susceptibility (11) of the solid or the direction-dependent magnetic excitation energies determined by inelastic neutron scattering experiments (12, 13). In this experimental approach the J parameters are obtained as numerical fitting parameters. Therefore, the J parameters of a magnetic solid deduced in particular from the magnetic susceptibility data of powder samples are difficult to relate to the crystal structure, although the latter provides an initial guess for the kinds of J parameters with which to begin the fitting procedure. For instance, the geometrical structures of the CuM_2O_6 (M = V, Nb) phases have edge-sharing CuO_4 chains, and one may fit their magnetic susceptibility data with a 1D Heisenberg AFM chain model to a first approximation. However, the magnetic chain directions may not be the same as the edge-sharing CuO_4 chain directions.

In the present work we probe how the 1D magnetic chains of CuM_2O_6 (M = Sb, V, Nb) are related to their crystal structures. In the following we analyze the reported crystal structures of CuM_2O_6 (M = Sb, V, Nb) to identify their "spin dimers" (i.e., structural units containing two adjacent spin sites) and determine the arrangements of their magnetic orbitals. We then calculate the spin orbital interaction energies for these spin dimers and examine how the magnitudes of these energies are related to the arrangements of the magnetic orbitals. Our analysis shows that the 1D magnetic chains of CuM_2O_6 (M = V, Nb) are quite different than their edge-sharing CuO_4 chains.

2. QUALITATIVE DESCRIPTION OF SPIN EXCHANGE INTERACTION

The spin exchange parameter J between adjacent spins in a spin dimer is related to the energy difference ΔE

[1] To whom correspondence should be addressed.

0022-4596/01 $35.00

between the triplet and singlet states of the corresponding spin dimer as $J = \Delta E = {}^1E - {}^3E$, where ${}^1E$ and ${}^3E$ are the total energies of the singlet nd triplet states, respectively (11, 14–16). In general, J is written as $J = J_F + J_{AF}$, where J_F and J_{AF} refer to the ferromagnetic and antiferromagnetic terms, respectively (i.e., $J_F > 0$ and $J_{AF} < 0$). The J values for transition metal oxides and fluorides of perovskite-type structures are well reproduced by the ΔE values of the corresponding spin dimers determined from first-principles electronic structure calculations (17). However, this total energy approach is difficult to apply to magnetic solids with large and complex unit cells. Recently we have shown (18–24) that the qualitative trends in the J parameters of a magnetic solid can be explained in terms of the spin orbital interaction energies calculated for their spin dimers using the extended Hückel method (25, 26). For the interaction between two crystallographically equivalent spin sites, $|J_{AF}|$ increases with increasing the spin orbital interaction energy Δe, where Δe is the energy separation between the two highest singly occupied energy levels of a spin dimer (Fig. 1a) (14). For the interaction between two crystallographically nonequivalent spin sites, $|J_{AF}|$ increases with increasing the energy $\sqrt{(\Delta e)^2 - (\Delta e^0)^2}$, where Δe^0 is the energy difference between the spin levels of the two spin monomers (i.e., the cluster units containing a single unpaired electron) comprising the spin dimer (Fig. 1b) (16, 21). The $\sqrt{(\Delta e)^2 - (\Delta e^0)^2}$ term increases with the net spin orbital interaction energy, $(\Delta e - \Delta e^0)$. (For the interaction between two equivalent spins, $\Delta e^0 = 0$.) When $(\Delta e - \Delta e^0)$ is negligible, the spin exchange interaction is expected to be ferromagnetic. For an AFM spin exchange interaction, the variation of J can be understood by studying that of the corresponding $(\Delta e - \Delta e^0)$ value.

3. STRUCTURES AND SPIN DIMERS OF CuM_2O_6

The spin monomers of CuM_2O_6 (M = Sb, V, Nb) are the octahedral clusters $(CuO_6)^{10-}$ containing Cu^{2+} (d^9) cations. Each CuO_6 octahedron shows an "axial" elongation of two *trans* Cu–O bonds due to a Jahn–Teller distortion. For convenience, the oxygen atoms of the two elongated Cu–O bonds will be referred to as the axial oxygen atoms, O_{ax}, and those of the remaining four Cu–O bonds of CuO_6 as the equatorial oxygen atoms, O_{eq}. If we choose the "idealized" local coordinate system for a distorted CuO_6 octahedron such that the Cu–O_{eq} bonds are pointed along the x- and y-axes (Fig. 2), then the unpaired spin of each $(CuO_6)^{10-}$ cluster resides in the magnetic orbital in which the x^2–y^2 orbitals of Cu and the $2p$ orbitals of O_{eq} are combined out of phase (27). The interaction between the adjacent magnetic orbitals of a spin dimer gives rise to the $(\Delta e - \Delta e^0)$ value of the spin dimer. Therefore, it is crucial to examine how the square planar Cu $(O_{eq})_4$ units containing the magnetic orbitals are spatially arranged in CuM_2O_6 (M = Sb, V, Nb). The MO_6 octahedra share their oxygen atoms with the CuO_6 octahedra, but the arrangements of the MO_6 octahedra are not discussed in the following for the sake of simplicity.

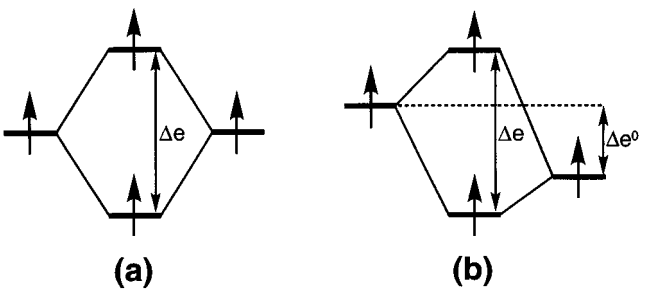

FIG. 1. Interaction between (a) equivalent spin monomers and (b) nonequivalent spin monomers of a spin dimer.

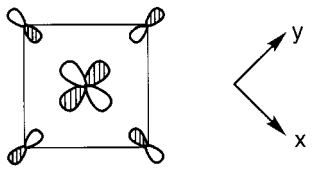

FIG. 2. Magnetic orbital of an axially elongated octahedral cluster $(CuO_6)^{10-}$, in which the $x^2 - y^2$ orbital of the Cu atom is combined out-of-phase with the p orbitals of the O_{eq} atoms.

Figure 3a shows a schematic view of a *trans*-edge-sharing CuO_4 chain made up of regular CuO_6 octahedra. As shown in Fig. 3b, the *trans*-edge-sharing CuO_4 chains of α-CuV_2O_6 have distorted CuO_6 octahedra, and the magnetic orbital planes of the CuO_6 octahedra are parallel to one another. Figure 3c shows a perspective view of a *cis*-edge-sharing CuO_4 chain made up of regular CuO_6 octahedra. The *cis*-edge-sharing CuO_4 chains of α-$CuNb_2O_6$ (Fig. 3d) and that of β-$CuNb_2O_6$ (Fig. 3e) have distorted CuO_6 octahedra. These *cis*-edge-sharing CuO_4 chains are different in the way the magnetic orbital planes are arranged. In order to facilitate the description of the 3D crystal structures of CuM_2O_6, we present the CuO_4 chains of Figs. 3a–3c as the projection views along the chain direction as depicted in Figs. 4a–4c, respectively.

$CuSb_2O_6$ has the trirutile structure type and has the *trans*-edge-sharing $CuSb_2O_{12}$ chain (Fig. 5a) as the structural building unit. For simplicity, the projection view of this chain along the c-direction may also be represented by Fig. 4a. The $CuSb_2O_{12}$ chains of $CuSb_2O_6$ are then arranged as shown in Figs. 5b and 5c at the c-axis heights $z = 0$ and $c/2$, respectively, such that the CuO_6 octahedra occur only on the ab-planes at the c-axis heights $z = 0$ and $c/2$. The CuO_6 octahedra of each $CuSb_2O_{12}$ chain are distorted as depicted in Fig. 3b, so that the magnetic orbital

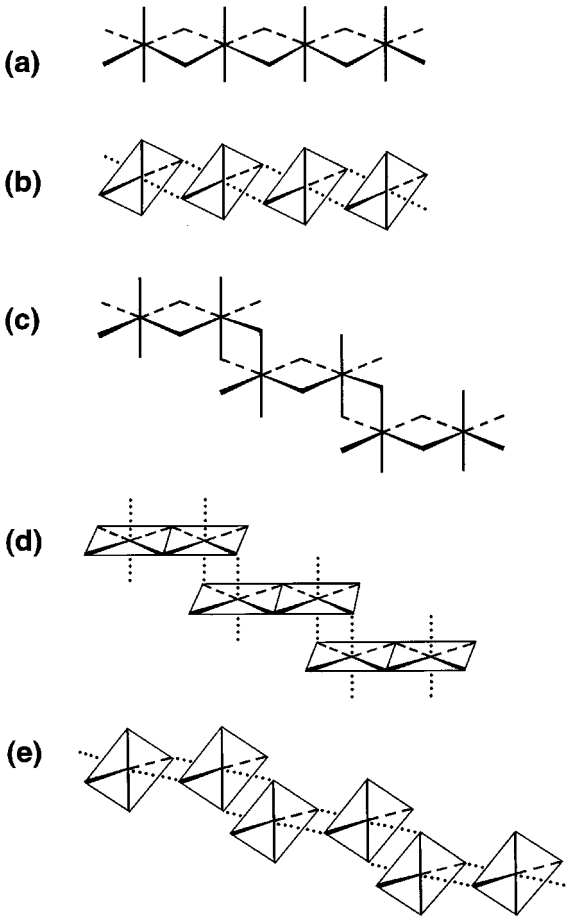

FIG. 3. Schematic views of *trans*-edge-sharing CuO_4 chains made up of (a) regular CuO_6 octahedra and (b) distorted CuO_6 octahedra. Schematic views of *cis*-edge-sharing CuO_4 chains made of (c) regular CuO_6 octahedra and (d, e) distorted CuO_6 octahedra.

planes of the distorted CuO_6 octahedra on the *ab*-planes of the *c*-axis heights $z = 0$ and $c/2$ are arranged as shown in Figs. 5d and 5e, respectively.

The *trans*-edge-sharing CuO_4 chains of α-CuV_2O_6 are arranged along the *b*-direction as shown in Fig. 6a. Thus, the magnetic orbital planes of the CuO_6 octahedra are arranged as depicted in Fig. 6b, where the middle two CuO_4 chains (along the *a*-direction) differ in the *b*-axis height from the other CuO_4 chains by $b/2$.

This is shown in the perspective view of the CuO_4 chains along the *c*-direction presented in Fig. 6c.

The arrangements of the *cis*-edge-sharing CuO_4 chains in α- and β-$CuNb_2O_6$ along the chain direction can be represented as shown in Fig. 7a in terms of the projection view of an ideal *cis*-edge-sharing CuO_4 chain (Fig. 3c). The perspective view of the two adjacent CuO_4 chains along the direction perpendicular to the chain is shown in Fig. 7b for β-$CuNb_2O_6$, and in Fig. 7c for α-$CuNb_2O_6$.

The spin monomers of CuM_2O_6 are $(CuO_6)^{10-}$ ions, so that the intrachain spin dimers (i.e., those within a CuO_4 chain) of CuM_2O_6 are given by $(Cu_2O_{10})^{16-}$ ions composed of two edge-sharing CuO_6 octahedra, and the interchain spin dimers (i.e., those between adjacent CuO_4 chains) of CuM_2O_6 by $(Cu_2O_{12})^{20-}$ ions composed of two isolated $(CuO_6)^{10-}$ ions. The interaction between the spin monomers of an interchain spin dimer can be affected by the MO_6 octahedra bridging the two spin monomers. To study this effect, an interchain spin dimer can be defined as the $(Cu_2O_{12})^{20-}$ ion plus all the MO_6 octahedra that link the two Cu^{2+} ions via Cu–O–*M*–O–Cu bridges.

4. RESULTS

Table 1 summarizes the parameters of the atomic orbitals used in our extended Hückel molecular orbital calculations for the $(\Delta e - \Delta e^0)$ values of various spin dimers. Note that the *d* orbitals of Cu and the *s*/*p* orbitals of O are represented by double-zeta Slater-type orbitals (28, 29), because such orbitals reproduce well the trends in the anisotropic spin exchange interactions of magnetic transition metal oxides and fluorides (18–24). The $(\Delta e - \Delta e^0)$ values calculated for the various spin dimers of CuM_2O_6 are listed in Table 2, which also summarizes the Cu–Cu distances of the spin dimers and the shortest O–O distance between the two $(CuO_6)^{10-}$ ions in each interchain spin dimer. In the present work, the $(\Delta e - \Delta e^0)$ values of the interchain spin dimers were calculated with and without such bridging MO_6 octahedra. It is important to comment on the relative merits of these $(\Delta e - \Delta e^0)$ values in analogy with our study of the vanadium pyrophosphate $(VO)_2P_2O_7$ (24). The $(\Delta e - \Delta e^0)$ values calculated for the spin dimers with and without the bridging PO_4 tetrahedra showed that the calculations with the bridging PO_4 tetrahedra overestimate the spin exchange interactions and hence are in poorer agreement

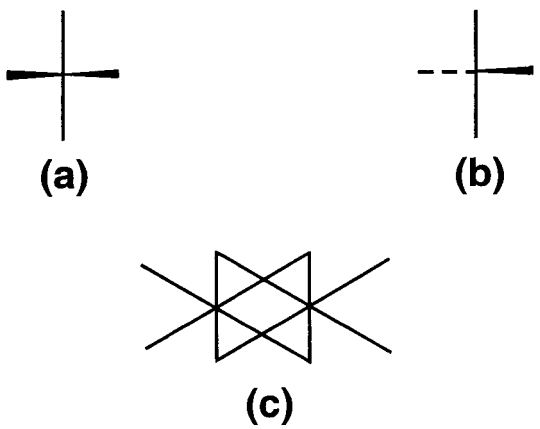

FIG. 4. Schematic projection views of the edge-sharing CuO_4 octahedral chains (along the chain direction) of (a) Fig. 3a, (b) Fig. 3b, and (c) Fig. 3c.

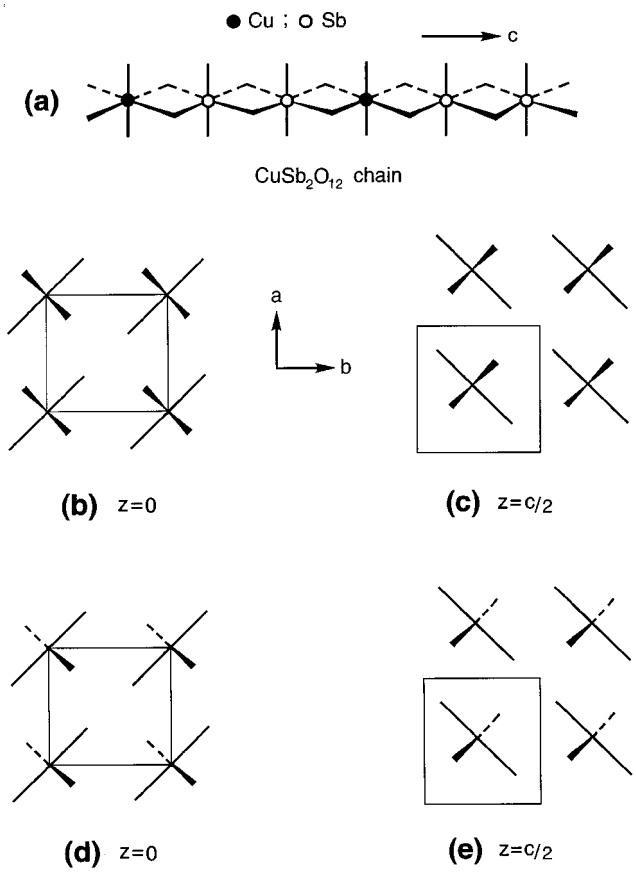

FIG. 5. Schematic description of the arrangement of the CuO_6 octahedra in $CuSb_2O_6$. (a) Perspective view of the $CuSb_2O_{12}$ chain. (b) Arrangement of the $CuSb_2O_{12}$ chains at the c-axis height $z = 0$. (c) Arrangement of the $CuSb_2O_{12}$ chains at the c-axis height $z = c/2$. (d) Arrangement of the magnetic orbital planes of the distorted CuO_6 octahedra at the c-axis height $z = 0$. (e) Arrangement of the magnetic orbital planes of the distorted CuO_6 octahedra at the c-axis height $z = c/2$.

with experiment than are those without the bridging PO_4 tetrahedra. This is due most likely to the fact that spin orbital interaction energies, being based on molecular orbital calculations, overemphasize delocalization when calculated with the V–O–P–O–V bridges. The same might be expected for our calculations of the interchain spin dimers with the Cu–O–M–O–Cu bridges. Therefore, the $(\Delta e - \Delta e^0)$ values calculated with the bridging MO_6 octahedra should be considered as overestimates, and the $(\Delta e - \Delta e^0)$ values appropriate for the interchain spin dimers should lie between the values calculated with and without the bridging MO_6 octahedra. This will be assumed to be the case in the following discussion of the $(\Delta e - \Delta e^0)$ values of Table 2.

$CuSb_2O_6$

In the layer of CuO_6 octahedra at the c-axis height $z = 0$, the $(\Delta e - \Delta e^0)$ value is largest in the $(a + b)$-direction, along which the $Cu(O_{eq})_4$ units have a coplanar arrangement (Fig. 5d) and have the shortest intermonomer $O \cdots O$ distance. The latter lead to a good sigma overlap between the adjacent magnetic orbitals (Fig. 2). The $(\Delta e - \Delta e^0)$ values are small in the a-, b- and $(a - b)$-directions, along which the $Cu(O_{eq})_4$ units are not coplanar and the overlap between adjacent magnetic orbitals is poor. Thus, the magnetic chains in this layer run along the $(a + b)$-direction. Likewise, in the layer of CuO_6 octahedra at the c-axis height $z = c/2$, the magnetic chains run along the $(a - b)$-direction (Fig. 5e). Consequently, $CuSb_2O_6$ consists of 1D magnetic chains although the Cu^{2+} ions form "square nets" in the layers of CuO_6 octahedra. The interaction between adjacent 1D magnetic chains is very weak compared with that within each 1D chain. This agrees with the experimental observation (1) that the interchain exchange interaction is significantly smaller than the intrachain exchange interaction (i.e., $|J| = \sim 0.086$ vs 43.1 K).

α-CuV_2O_6

The $(\Delta e - \Delta e^0)$ value is largest in the c-direction, along which the adjacent magnetic orbitals make a good sigma

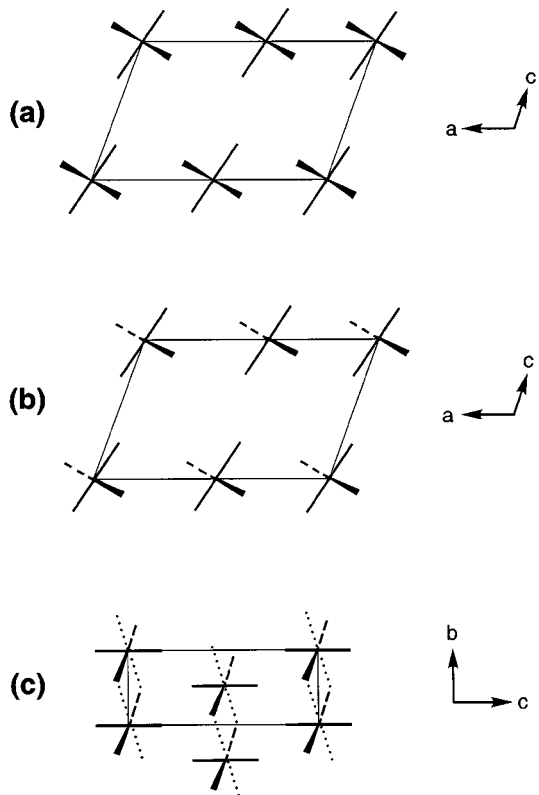

FIG. 6. Schematic description of the arrangement of the CuO_6 octahedra in α-CuV_2O_6. (a) Projection view of the *trans*-edge-sharing CuO_4 chains along the b-direction. (b) Arrangement of the magnetic orbital planes of the CuO_6 octahedra viewed along the b-direction. (c) Arrangement of the *trans*-edge-sharing CuO_4 chains viewed along the a-direction.

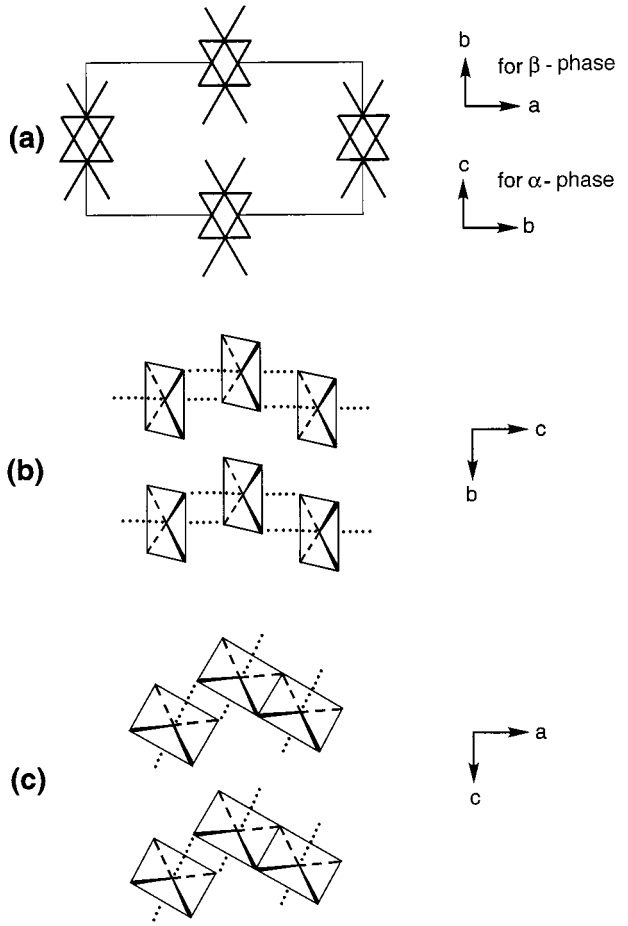

FIG. 7. Schematic description of the arrangement of the CuO_6 octahedra in α-$CuNb_2O_6$ and β-$CuNb_2O_6$. (a) Arrangements of the *cis*-edge-sharing CuO_4 chains in α- and β-$CuNb_2O_6$ along the chain direction. (b) Arrangement of the two adjacent CuO_4 chains in β-$CuNb_2O_6$ viewed along the *a*-direction. (c) Arrangement of the two adjacent CuO_4 chains in α-$CuNb_2O_6$ viewed along the *b*-direction.

overlap through the shortest O–O contact (Fig. 6b). The $(\Delta e - \Delta e^0)$ values are smaller in the *a*- and *b*-directions because the adjacent magnetic orbitals make a poor overlap. Thus, the 1D magnetic chains of α-CuV_2O_6 run along the *c*-direction and do not correspond to the *trans*-edge-sharing CuO_4 chains along the *b*-direction. Nevertheless, the interaction between adjacent 1D magnetic chains is substantial, which is consistent with the experimental finding (3) that the interchain exchange interactions are rather large compared with the intrachain exchange interaction (i.e., $|J|$ 16.5 vs 34 K).

β-CuNb₂O₆

The $(\Delta e - \Delta e^0)$ value is largest for the interchain spin dimer in the *b*-direction, along which the adjacent magnetic orbitals can have a good sigma overlap (Fig. 7b). The

TABLE 1

Exponents ζ_i and Valence Shell Ionization Potentials H_{ii} of Slater-type Orbitals χ_i Used for Extended Hückel Tight-Binding Calculation[a]

Atom	χ_i	H_{ii} (eV)	ζ_i	c_1^b	ζ_i'	c_2^b
Cu	4*s*	− 11.4	2.151	1.0		
Cu	4*p*	− 6.06	1.370	1.0		
Cu	3*d*	− 14.0	7.025	0.4473	3.004	0.6978
V	4*s*	− 8.81	1.697	1.0		
V	4*p*	− 5.52	1.260	1.0		
V	3*d*	− 11.0	5.052	0.3738	2.173	0.7456
Nb	5*s*	− 10.1	1.877	1.0		
Nb	5*p*	− 6.86	1.320	1.0		
Nb	4*d*	− 12.1	3.774	0.4583	1.925	0.6787
Sb	5*s*	− 18.8	2.959	0.6466	1.771	0.5018
Sb	5*p*	− 11.7	2.559	0.5610	1.474	0.5633
O	2*s*	− 32.3	2.688	0.7076	1.675	0.3745
O	2*p*	− 14.8	3.694	0.3322	1.659	0.7448

[a] H_{ii}'s are the diagonal matrix elements $\langle \chi_i | H^{\text{eff}} | \chi_i \rangle$, where H^{eff} is the effective Hamiltonian. In our calculations of the off-diagonal matrix elements $H_{\text{eff}} = \langle \chi_i | H^{\text{eff}} | \chi_j \rangle$, the weighted formula was used. See: J. Ammeter, H.-B. Bürgi, J. Thibeault, and R. Hoffmann, *J. Am. Chem. Soc.* **100,** 3686 (1978).

[b] Coefficients used in the double-zeta Slater-type orbital expansion.

$(\Delta e - \Delta e^0)$ values are smaller in the *a*- and *c*-directions, because the adjacent magnetic orbitals have a poor overlap. Thus, β-$CuNb_2O_6$ has 1D magnetic chains running in the *b*-direction, which are different from the *cis*-edge-sharing CuO_4 chains along the *c*-direction. This is consistent with the experimental observation that β-$CuNb_2O_6$ shows a 1D short-range AFM ordering with $T_M = 20$ K (8). Since the strongest AFM interaction takes place along the *b*-direction, the associated AFM ordering would make the magnetic unit cell double the unit cell along the *b*-direction as found for the CuM_2O_6 (M = Fe, Co, Ni) phases (30, 31), which are isomorphic with β-$CuNb_2O_6$. This prediction is in apparent disagreement with the recent powder neutron diffraction study (9), which reported that the spin exchange interaction is AFM within each *cis*-edge-sharing CuO_4 chain, and is ferromagnetic along the *b*-direction. However, the poor *R*-factor ($\sim$12%) of this neutron diffraction data makes it difficult to unequivocally conclude from the reported neutron diffraction profile either the absence of weak (1 0 1) and (2 1 0) magnetic reflections (needed to assign an AFM spin exchange interaction within each *cis*-edge-sharing chain) or that of weak $(0\,\frac{1}{2}\,0)$ reflections (needed to assign a ferromagnetic spin exchange interaction along the *b*-direction). A more accurate neutron diffraction study is required to resolve this issue.

α-CuNb₂O₆

The $(\Delta e - \Delta e^0)$ value is largest for the intrachain spin dimer in which the two $Cu(O_{eq})_4$ units are coplanar (Fig. 7c).

TABLE 2
($\Delta e - \Delta e^0$) Values (in me V), Cu–Cu Distances (in Å), and O–O Distances (in Å) of the Spin Dimers in CuM_2O_6 (M = Sb, V, Nb)

Compound	Direction[b]	Cu–Cu	O–O	$(\Delta e - \Delta e^0)$[c]
$CuSb_2O_6$[a]	a	4.635	2.784	21 (15)
	b	4.637	2.860	15 (5)
	$a+b$	6.556	2.551	164 (160)
	$a-b$	6.556	3.964	2 (1)
α-CuV_2O_6	b (intra)	3.543	—	34
	a (inter)	4.860	2.682	3 (54)
	c (inter)	6.478	2.756	85 (64)
β-$CuNb_2O_6$	c (intra)	3.196	—	9
	b (inter)	4.501	2.808	23 (35)
		5.613	2.857	85 (118)
	$a+b$ and $a-b$ (inter)	7.553	4.572	0
		7.587	4.572	1
α-$CuNb_2O_6$	a (intra)	3.050	—	67
		3.140	—	5
	c (inter)	4.608	2.790	6 (12)
		4.729	2.766	1 (16)
		5.762	2.766	12 (54)
	$b+c$ and $b-c$ (inter)	7.581	4.587	1

[a] In the layer of CuO_6 octahedra at the c-axis height $z = 0$.
[b] The entries "intra" and "inter" refer to "intrachain" and "interchain" spin dimers, respectively (with respect to the edge-sharing CuO_4 chains).
[c] The values with and without parentheses refer to those calculated with and without the MO_6 octahedra providing the Cu–O–M–O–Cu bridges, respectively.

The interchain spin dimer is substantial along the c-direction, and is negligible along the b-direction. Thus, in α-$CuNb_2O_6$ the spin dimers having the largest $(\Delta e - \Delta e^0)$ value interact substantially along the c-direction. This gives rise to alternating 1D AFM chains running along the c-direction, which differ from the *cis*-edge-sharing CuO_4 chains. Our result is consistent with the experimental observation that the magnetic susceptibility of α-$CuNb_2O_6$ is better described by an alternating 1D AFM chain model (10) than by an isolated spin dimer model (5).

5. CONCLUDING REMARKS

The present study shows that the observed magnetic anisotropy of the CuM_2O_6 (M = Sb, V, Nb) phases is well explained in terms of the spin orbital interaction energies $(\Delta e - \Delta e^0)$ calculated for their spin dimers. The magnetic orbital of each Cu^{2+} site in CuM_2O_6 is given by the x^2-y^2 orbital of the square planar $Cu(O_{eq})_4$ unit containing the Cu^{2+} ion. Thus, the magnitude of the interaction between two adjacent magnetic orbitals is large, and hence the corresponding AFM spin exchange interaction becomes strong, when the arrangement of the adjacent square planar $Cu(O_{eq})_4$ units provides a good sigma overlap between the magnetic orbitals through the shortest Cu–O–O–Cu contact. The 1D magnetic chains of α-CuV_2O_6, β-$CuNb_2O_6$, and α-$CuNb_2O_6$ run along the direction different than their edge-sharing CuO_4 chain directions. It would be interesting to test our prediction that the AFM ordering in β-$CuNb_2O_6$ should make the magnetic unit cell double the chemical unit cell along the b-direction.

ACKNOWLEDGMENTS

Work at North Carolina State University was supported by the Office of Basic Energy Sciences, Division of Materials Sciences, U.S. Department of Energy, under Grant DE-FG05-86ER45259.

REFERENCES

1. A. Nakua, H. Yun, J. N. Reimers, J. E. Greedan, and C. V. Stager, *J. Solid State Chem.* **91,** 105 (1991) and references cited therein.
2. C. Calvo and D. Manolescu, *Acta Crystallogr. B* **29,** 1743 (1973).
3. A. N. Vasil'ev, L. A. Ponomarenko, A. I. Smirnov, E. V. Antipov, Yu. A. Velikodny, M. Isobe, and Y. Ueda, *Phys. Rev. B* **60,** 3021 (1999).
4. H. Kasper, *Rev. Chim. Miner.* **4,** 759 (1967).
5. E. Wahlström and B.-O. Marinder, *Inorg. Nucl. Chem. Lett.* **13,** 559 (1977).
6. J. Norwig, H. Weitzel, H. Paulus, G. Lautenschlager, J. Rodriguez-Carvajal, and H. Fuess, *J. Solid State Chem.* **115,** 476 (1995).
7. E. J. Felten, *J. Inorg. Nucl. Chem.* **29,** 1168 (1967).
8. M. G. B. Drew, R. J. Hobson, and V. T. Padayatcy, *J. Mater. Chem.* **3,** 889 (1993).
9. S. Mitsuda, J. Miyamoto, S. Kobayashi, K. Miyatani, and T. Tanaka, *J. Phys. Soc. Jpn.* **67,** 1060 (1998).
10. K. Kodama, T. Fukumachi, H. Harashina, M. Kanada, Y. Kobayashi, M. Kasai, H. Sasaki, M. Sato, and K. Kakurai, *J. Phys. Soc. Jpn.* **67,** 57 (1998).
11. O. Kahn, "Molecular Magnetism." VCH, Weinheim, 1993.
12. S. Taniguchi, T. Nishikawa, Y. Yasui, Y. Kobayashi, M. Sato, T. Nishioka, M. Kontani, and K. Sano, *J. Phys. Soc. Jpn.* **64,** 2758 (1996).
13. A. W. Garret, S. E. Nagler, D. A. Tennant, B. C. Sales, and T. Barnes, *Phys. Rev. Lett.* **79,** 745 (1997).
14. P. J. Hay, J. C. Thibeault, and R. Hoffmann, *J. Am. Chem. Soc.* **97,** 4884 (1975).
15. O. Kahn and B. Briat, *J. Chem. Soc., Faraday Trans. 2* **72,** 268 (1976).
16. O. Kahn, *Struct. Bonding* **68,** 89 (1987).
17. F. Illas, I. de P. R. Moreira, C. de Graaf, and V. Barone, *Theor. Chem. Acc.*, in press, and references cited therein.
18. K.-S. Lee, H.-J. Koo, and M.-H. Whangbo, *Inorg. Chem.* **38,** 2199 (1999).
19. H.-J. Koo and M.-H. Whangbo, *Solid State Commun.* **111,** 353 (1999).
20. H.-J. Koo and M.-H. Whangbo, *J. Solid State Chem.* **151,** 96 (2000).
21. M.-H. Whangbo, H.-J. Koo, and K.-S. Lee, *Solid State Commun.* **114,** 27 (2000).
22. M.-H. Whangbo and H.-J. Koo, *Solid State Commun.* **115,** 675 (2000).
23. H.-J. Koo and M.-H. Whangbo, *J. Solid State Chem.* **153,** 263 (2000).

24. H.-J. Koo and M.-H. Whangbo, *Inorg. Chem.* **39,** 3599 (2000).
25. R. Hoffmann, *J. Chem. Phys.* **39,** 1397 (1963).
26. Our calculations were carried out by employing the CAESAR program package. J. Ren, W. Liang, and M.-H. Whangbo, "Crystal and Electronic Structure Analysis Using CAESAR," 1998. This book can be downloaded free of charge from the Web site http://www.PrimeC.com/.
27. T. A. Albright, J. K. Burdett, and M.-H. Whangbo, "Orbital Interactions in Chemistry." Wiley, New York, 1985.
28. E. Clementi and C. Roetti, *Atomic Data Nuclear Data Tables* **14,** 177 (1974).
29. A. D. McLean and R. S. McLean, *Atomic Data Nuclear Data Tables* **26,** 197 (1981).
30. S. Mitsuda, S. Kobayashi, K. Aga, H. Katagiri, H. Yoshizawa, M. Ishikawa, K. Miyatani, and K. Kohn, *J. Phys. Soc. Jpn.* **64,** 2325 (1995).
31. O. V. Nielson, B. Lebech, F. K. Larsen, L. M. Holmes, and A. A. Ball, *J. Phys. C*: *Solid State Phys.* **9,** 2401 (1976).